

Ab initio kinetics and thermal decomposition mechanism of mononitrobiuret and 1,5-dinitrobiuret

Hongyan Sun and Ghanshyam L. Vaghjiani

Citation: *The Journal of Chemical Physics* **142**, 204301 (2015); doi: 10.1063/1.4921378

View online: <http://dx.doi.org/10.1063/1.4921378>

View Table of Contents: <http://scitation.aip.org/content/aip/journal/jcp/142/20?ver=pdfcov>

Published by the AIP Publishing

Articles you may be interested in

Reaction mechanisms and kinetics of the iminovinylidene radical with NO: Ab initio study
J. Chem. Phys. **140**, 204316 (2014); 10.1063/1.4876015

Theoretical study on reaction mechanism and kinetics of HNCS with CN
J. Chem. Phys. **139**, 154307 (2013); 10.1063/1.4825080

Correlated ab initio investigations on the intermolecular and intramolecular potential energy surfaces in the ground electronic state of the O₂ – (XΠg₂) – HF (XΣ+1) complex
J. Chem. Phys. **138**, 014304 (2013); 10.1063/1.4772653

Product branching ratios in photodissociation of phenyl radical: A theoretical ab initio/Rice–Ramsperger–Kassel–Marcus study
J. Chem. Phys. **136**, 234305 (2012); 10.1063/1.4726455

Ab initio investigation of titanium hydroxide isomers and their cations, TiOH₀, + and HTiO₀, +
J. Chem. Phys. **135**, 144111 (2011); 10.1063/1.3644963



NEW Special Topic Sections

NOW ONLINE
Lithium Niobate Properties and Applications:
Reviews of Emerging Trends

**AIP | Applied Physics
Reviews**

Ab initio kinetics and thermal decomposition mechanism of mononitrobiuret and 1,5-dinitrobiuret

Hongyan Sun^{a)} and Ghanshyam L. Vaghjiani^{a)}

Propellants Branch, Rocket Propulsion Division, Aerospace Systems Directorate, Air Force Research Laboratory, AFRL/RQRP, 10 E. Saturn Blvd., Edwards AFB, California 93524, USA

(Received 4 March 2015; accepted 8 May 2015; published online 26 May 2015)

Mononitrobiuret (MNB) and 1,5-dinitrobiuret (DNB) are tetrazole-free, nitrogen-rich, energetic compounds. For the first time, a comprehensive *ab initio* kinetics study on the thermal decomposition mechanisms of MNB and DNB is reported here. In particular, the intramolecular interactions of amine H-atom with electronegative nitro O-atom and carbonyl O-atom have been analyzed for biuret, MNB, and DNB at the M06-2X/aug-cc-pVTZ level of theory. The results show that the MNB and DNB molecules are stabilized through six-member-ring moieties via intramolecular H-bonding with interatomic distances between 1.8 and 2.0 Å, due to electrostatic as well as polarization and dispersion interactions. Furthermore, it was found that the stable molecules in the solid state have the smallest dipole moment amongst all the conformers in the nitrobiuret series of compounds, thus revealing a simple way for evaluating reactivity of fuel conformers. The potential energy surface for thermal decomposition of MNB was characterized by spin restricted coupled cluster theory at the RCCSD(T)/cc-pV ∞ Z//M06-2X/aug-cc-pVTZ level. It was found that the thermal decomposition of MNB is initiated by the elimination of HNCO and HNN(O)OH intermediates. Intramolecular transfer of a H-atom, respectively, from the terminal NH₂ group to the adjacent carbonyl O-atom via a six-member-ring transition state eliminates HNCO with an energy barrier of 35 kcal/mol and from the central NH group to the adjacent nitro O-atom eliminates HNN(O)OH with an energy barrier of 34 kcal/mol. Elimination of HNN(O)OH is also the primary process involved in the thermal decomposition of DNB, which processes C_{2v} symmetry. The rate coefficients for the primary decomposition channels for MNB and DNB were quantified as functions of temperature and pressure. In addition, the thermal decomposition of HNN(O)OH was analyzed via Rice–Ramsperger–Kassel–Marcus/multi-well master equation simulations, the results of which reveal the formation of (NO₂ + H₂O) to be the major decomposition path. Furthermore, we provide fundamental interpretations for the experimental results of Klapötke *et al.* [Combust. Flame 139, 358–366 (2004)] regarding the thermal stability of MNB and DNB, and their decomposition products. Notably, a fundamental understanding of fuel stability, decomposition mechanism, and key reactions leading to ignition is essential in the design and manipulation of molecular systems for the development of new energetic materials for advanced propulsion applications. [<http://dx.doi.org/10.1063/1.4921378>]

I. INTRODUCTION

In the search for energetic materials for explosives and propellants for military and civilian applications, many compounds have been designed and synthesized to provide increased energy density performance, high thermal stability, and better oxygen balance. For example, aza-heterocyclic nitramines like cyclotrimethylene trinitramine (RDX) or cyclotetramethylene tetranitramine (HMX), and nitro-aromatics like 2,4,6-trinitrotoluene (TNT) are being used widely because of their high energy densities and excellent detonation properties. To improve the safety in handling of explosives, the search for new energetic materials is certainly merited. The RDX and HMX analogues such as mononitrobiuret (MNB, C₂H₄N₄O₄) and 1,5-dinitrobiuret (DNB, C₂H₃N₅O₆), which preserve the nitrourea moiety in a cyclic structure, have

been sought to meet the requirements of increased thermal stability and insensitivity, as well as performance. Klapötke *et al.* synthesized and investigated the thermal decomposition of MNB and DNB by thermo-gravimetric analysis and differential scanning calorimetry.^{1,2} MNB was synthesized by nitration of biuret with HNO₃/H₂SO₄, and DNB was obtained by the treatment of MNB with 100% HNO₃ using a modified procedure of Thiele,³ with an overall yield of 46% from the starting biuret.^{1,4} They observed that both MNB and DNB were white solids and MNB decomposed without melting at 153 °C, while DNB exploded when heated above 127 °C. In addition, DNB was observed to be impact and heat sensitive, had a density of 1.859 g/cm³, and detonated strongly without an oxidizer in a steel-sleeve test after 4 s.² Furthermore, they found that MNB and DNB showed distinctively different thermal behaviors, i.e., MNB had a significantly higher decomposition temperature than DNB and as such, was found to have better thermal stability. Using mass spectrometry and IR spectroscopy, they identified the gaseous products

^{a)}Authors to whom correspondence should be addressed. Electronic addresses: hongyan.sun1@gmail.com and ghanshyam.vaghjiani@us.af.mil

from the decomposition of MNB and DNB and proposed a reaction scheme to interpret their observations. In particular, they suggested that the thermal decomposition of MNB and DNB is initiated by the release of nitramine (NH_2NO_2), which decomposes to dinitrogen oxide (N_2O) and water. After this initiation step, the residue of MNB decomposes directly into two isocyanic acid (HNCO) molecules, while the residue of DNB leads directly to HNCO, N_2O , and CO_2 .

Recently, quasi-classical direct dynamics trajectory simulations have been performed to get a better understanding of the decomposition mechanism in DNB.^{5,6} In these studies, the elimination of HNN(O)OH intermediate via a concerted mechanism was identified as a dominant channel for DNB thermal decomposition. Here, it is noted that HNN(O)OH has a geometry in which the OH group is *trans* to the NH group along the N—N bond and *trans* to the N=O group along the N—OH bond.

To further understand the thermal stability and explosive behavior of MNB and DNB, we have investigated their thermal decomposition reaction mechanisms using advanced *ab initio* quantum chemistry and kinetics theories. In this paper, we present the molecular structures of MNB and DNB starting with the backbone structure of the biuret molecule to elucidate structure-dependent molecular properties. Conformational isomerism and molecular properties of the conformers were analyzed to understand their solid-state stabilities. The potential energy surfaces (PESs) for the thermal decomposition of MNB and DNB molecules, and intermediates were characterized to interpret the intermediates and products formation observed in previous pyrolysis experiments.¹ Temperature and pressure-dependent rate coefficients were calculated using micro-canonical transition state theory with master equation simulations to provide quantitative interpretations of the thermal stability, products formation, and explosive behavior.

II. THEORETICAL METHODOLOGIES

A. Molecular structures and PESs

MNB and DNB are poly-nitrogen and poly-oxygen containing molecules. For such systems, non-covalent interactions from electrostatics as well as dispersion play an important role in determining both the structure and energy. It is recognized that the popular density functional such as the B3LYP fails to accurately represent London dispersion interactions.⁷ However, on the other hand, the new functional such as the M06-2X,⁸ which is a global hybrid functional with 54% HF exchange functional, has been proved highly successful for calculating non-covalent and dispersion interaction energies in neutral molecular systems, as well as for situations involving large molecules and also in solid-state physics.⁹ For the systems studied here, we found that for the species with C_s symmetry, the molecular structures were planar when using M06-2X optimization but non-planar with B3LYP optimization. In particular, the M06-2X optimization predicted DNB to possess C_{2v} symmetry, which is consistent with the experimental observation of the crystalline state.¹ Consequently, for the species involved in the initial decomposition

of MNB and DNB, spin restricted or unrestricted M06-2X method with Dunning's augmented correlation-consistent, polarized-valence double- ζ , and also triple- ζ basis sets (aug-cc-pVDZ and aug-cc-pVTZ)^{10,11} was applied to optimize the geometries and then to calculate the ro-vibrational frequencies for the species involved in MNB and DNB reaction systems.

As mentioned above and further discussed below, HNN(O)OH is an important intermediate formed directly from the primary channels of MNB and DNB thermal decomposition, which undergoes further decomposition to produce active radicals and stable products. For the species involved in HNN(O)OH decomposition, several advanced *ab initio* methods were applied for calculating geometries and ro-vibrational frequencies. In particular, the CCSD(T)/aug-cc-pCVTZ method was applied for small species containing up to 3 atoms and the CCSD(T)-F12/cc-pVTZ-F12 method was applied for the decomposition products containing more than 3 atoms. For HNN(O)OH isomers and their transition states, complete active space perturbation theory at the CASPT2/aug-cc-pVDZ level was applied since we have found that multi-reference second-order perturbation theory⁵ predicts remarkably accurate molecular geometries and vibrational frequencies for nitrogen and oxygen containing species.¹² For the active space, 12 electrons distributed amongst 9 orbitals were found to be adequate, i.e., four σ orbitals including bonding and antibonding pairs of N—N and N—OH bonds, the π bonding orbitals of N=O double bond, the π antibonding orbitals among all the heavy atoms, and three hybrid p orbitals on nitric oxygen, hydroxy oxygen, and amino nitrogen, respectively. For the transition state for N—OH bond fission, the state-averaged active space (4e, 3o) was chosen, which consisted of two degenerate p orbitals of OH and the p orbitals of N-atoms.

All of the reaction pathways were verified by the intrinsic reaction coordinate (IRC) analysis or relaxed bond scan methods. Higher-level (HL) single point energies were further obtained from spin restricted coupled-cluster theories with single and double excitations, and corrections for triple excitations, with cc-pVTZ and cc-pVQZ basis sets extrapolated to the complete basis set limit (CBS). The RHF-RCCSD(T)/CBS(TZ, QZ) energies for the HNN(O)OH system were then extrapolated by the asymptotic form.^{13,14} For nitrobiuret systems, the CCSD(T) calculation with cc-pVQZ basis set is a formidable task; therefore, the energies at the cc-pV ∞ Z limit were extrapolated by a modified asymptotic form,¹⁵ where the RCCSD(T) calculations employed the cc-pVDZ and cc-pVTZ basis sets, and the spin restricted Møller-Plesset perturbation (RMP2) RMP2 calculations employed the double- ζ (cc-pVDZ), triplet- ζ (cc-pVTZ), and quadruple- ζ (cc-pVQZ) basis sets. All electronic structure calculations were performed using Gaussian09¹⁶ and MOLPRO¹⁷ quantum chemistry packages.

B. Temperature and pressure-dependent kinetics

For reaction channels with well-defined transition states, the high-pressure rate coefficients were obtained from transition state theory (TST) employing rigid-rotor harmonic-oscillator assumptions for all degrees of freedom except the

torsional ones. Hindered rotor corrections for the torsional modes were obtained from one-dimensional fits to the torsional potentials employing Pitzer-Gwinn like approximations and the $I^{(2,3)}$ moments of inertia.¹⁸ For reactions with submerged energy barriers, the two-transition-state model proposed by Georgievskii and Klippenstein¹⁹ was applied to determine the rate coefficients, especially at low to intermediate temperatures. For bond fission reactions without any reverse energy barriers, rate coefficients were determined by inverse Laplace transformation²⁰ with reverse rate coefficients and reaction enthalpies. Tunneling corrections were included for all transition states based on the asymmetric Eckart potentials,²¹ with the parameters for the potentials computed from the imaginary frequency of the transition state and the forward and reverse barrier heights, where the energies of H-bonded product complexes are used for determining reverse barrier heights.

For PESs consisting of multiple, interconnected potential wells, and multiple product channels, the phenomenological thermal decomposition rate coefficients were determined by using Rice–Ramsperger–Kassel–Marcus (RRKM) theory together with the multi-well master equation simulations developed by Miller and Klippenstein,^{22–24} which are implemented in the VariFlex code.²⁵ The collisional energy transfer probability in the master equation analysis was approximated by single-exponential-down models for the average downward energy transfer. The Lennard-Jones parameters for collision rates were estimated by the group contribution method that correlates the critical temperature of a substance with its normal boiling point and critical pressure.²⁶ They were determined to be $\sigma = 5.3 \text{ \AA}$ and $\epsilon = 642 \text{ cm}^{-1}$ for MNB, $\sigma = 5.6 \text{ \AA}$ and $\epsilon = 781 \text{ cm}^{-1}$ for DNB, and $\sigma = 4.45 \text{ \AA}$ and $\epsilon = 379.3 \text{ cm}^{-1}$ for HNN(O)OH isomers. The Lennard-Jones parameters of $\sigma = 3.70 \text{ \AA}$ and $\epsilon = 66.1 \text{ cm}^{-1}$ were adopted for nitrogen.²⁷

III. RESULTS AND DISCUSSIONS

A. Molecular structures of MNB and DNB

For the MNB and DNB samples used in the pyrolysis experiments of Klapötke *et al.*,¹ the materials were characterized by IR, Raman, and NMR spectroscopy, and single crystal X-ray diffraction. They reported that the DNB molecule in the crystalline state had a planar structure with C_{2v} symmetry.² For MNB, the crystal structure was found to be non-planar, where the nitramine moiety was slightly rotated out of the biuret backbone plane, with a corresponding torsion angle, $\angle O—C—N—N(O_2)$ of 157.73° .⁴

As the backbone of MNB and DNB, the biuret geometry is crucial in understanding the molecular structures of its nitrosubstitutes. Biuret has been known to have two conformers, *trans* and *cis*, which refer to the two C=O groups that are either *trans* or *cis* to each other. Figure 1 shows the geometries of biuret (*trans*) and biuret (*cis*) optimized at the M06-2X/aug-cc-pVTZ level of theory. It is seen that, in biuret (*trans*), an amine H-atom interacts with its adjacent carbonyl O-atom with an intra-atomic distance of 1.945 \AA that forms an intramolecular N—H···O hydrogen bond along a

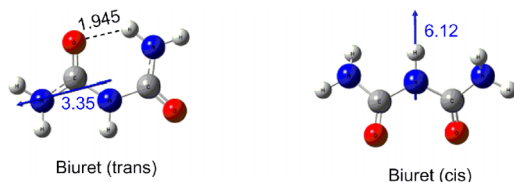


FIG. 1. Molecular structures of biuret conformers optimized at the M06-2X/aug-cc-pVTZ level. Intra-atomic distance for H-bonding is in Å. The dipole moment vector (blue) starts from the center of nuclear charge, unit in D. For biuret (*cis*), the dipole moment vector is scaled by a factor of 0.5.

six-member-ring moiety. Furthermore, the molecule is non-planar and the dihedral angle between the two C=O groups is 8.48° . While for biuret (*cis*), the molecular plane is more bent, the dihedral angle between the two C=O groups is 33.62° due to the repulsion between the carbonyl oxygen atoms, where the intra-atomic distance is 2.90 \AA . In addition, it was found that biuret (*cis*) is 11.65 kcal/mol higher in energy than biuret (*trans*) due to repulsion between the carbonyl oxygen atoms and also due to lack of stabilization via intramolecular H-bonding. The crystal structure of biuret hydrate established by Hughes *et al.*²⁸ shows that the biuret molecules lie in slightly buckled sheets, with each molecule being joined to three neighboring molecules by N—H···O hydrogen bonds. Furthermore, the two planar amide fragments ($\text{NH}_2—\text{CO—NH}$) in the biuret molecule are slightly inclined at $5^\circ 33'$ and *trans* to each other, forming an intramolecular H-bond. Notably, water in the biuret hydrate has some effect on its molecular structure, but a six-member-ring moiety with intramolecular N—H···O hydrogen bonding is a key factor for the stability of solid-state biuret.

With this in mind, we found four MNB conformations and three DNB conformations possessing intramolecular H-bonds and six-member-ring moieties, as depicted in Figures 2 and 3. Specifically, the conformers MNB (C_s), MNB (C_1), and MNB (*trans*) with the NO₂ substituted for the terminal amino H-atom conserve the six-member-ring moiety in the biuret. For the MNB (*cis*) conformer, it is the NO₂ substitution of an amino H-atom of biuret (*cis*) that forms a new intramolecular H-bond between a nitro O-atom and the central amino H-atom. For the DNB (C_s) conformer, it is the NO₂ substitution of a H-atom of NH₂ in MNB (C_s) and MNB (*trans*), which not only conserves the original six-member-ring moiety but also forms a new H-bond with another six-member-ring moiety. The DNB (C_1) and DNB (C_{2v}) conformers result from the NO₂ substitution of each of the H-atoms of NH₂ in MNB (*cis*).

From the energies of these conformers, it was found that the MNB (C_s) was the lowest energy conformer with a planar structure and C_s symmetry since it not only conserves the six-member-ring moiety of the biuret with a N—H···O hydrogen bond of 1.974 \AA but also forms a new six-member-ring moiety with an intramolecular H-bond of 1.953 \AA between a nitro O-atom and the central amino H-atom for extra stabilization. On the contrary to the MNB (C_s) conformer, the MNB (C_1) conformer results from NO₂ substitution of the other amino H-atom of the same NH₂ group, and because of the repulsion between the carbonyl O-atom and nitro O-atom, the —NHNO₂ group slightly rotates out of the biuret backbone plane with a corresponding torsion angle, $\angle N—C—N—NO_2$

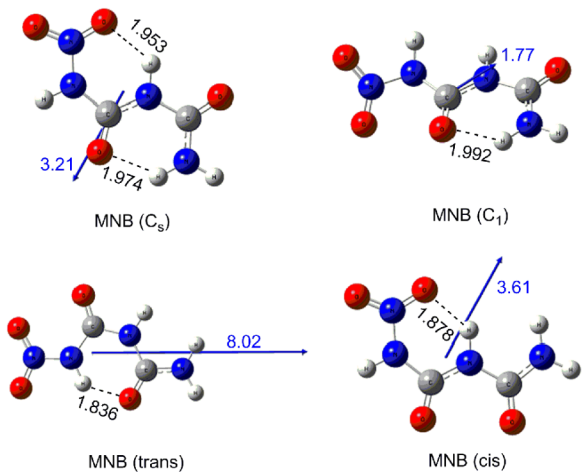


FIG. 2. Molecular structures of MNB conformers optimized at the M06-2X/aug-cc-pVTZ level. Intra-atomic distance for H-bonding is in Å. The dipole moment vector (blue) starts from the center of nuclear charge, unit in D.

of 178.20° . The MNB (*trans*) and MNB (*cis*) conformers were found to be planar. Relative to MNB (C_s), the conformers MNB (C_1), MNB (*trans*), and MNB (*cis*), respectively, have energies of 6.38, 4.82, and 7.95 kcal/mol, at the M06-2X/aug-cc-pVTZ level of theory.

The electronic structure of DNB was recently studied by Dorofeeva *et al.*²⁹ by two-dimensional B3LYP potential energy scans. They reported two low-energy conformers, named as pseudo-*trans* (C_s) and pseudo-*cis* (C_2), which differed in energy by 1.8 kcal/mol from the G4 calculations. Here, we found that DNB with C_2 symmetry exists in higher symmetry conformation of C_{2v} . Figure 3 shows three DNB conformers, DNB (C_s), DNB (C_1), and DNB (C_{2v}), optimized at the M06-2X/aug-cc-pVTZ level of theory. DNB (C_s) and DNB (C_{2v}) are the two low-energy conformers which are stabilized with two intramolecular H-bonds, which have interatomic distances of ca. 1.9 Å. Furthermore, we have found that DNB (C_s) is 1.22 kcal/mol lower in energy compared to DNB (C_{2v}), which can be ascribed to two facts: (a) one of its six-member-ring moieties is stabilized with a H-bond having a shorter interatomic distance of 1.891 Å between the amino H-atom and carbonyl O-atom, and (b) the interatomic distance between the two adjacent nitro O-atoms in DNB (C_{2v}) is 3.0 Å; hence, the electrostatic repulsion between them increases the energy of C_{2v} isomer. For DNB (C_1), which is a rotamer of DNB (C_s) or DNB (C_{2v}), its energy is 7.82 kcal/mol higher than that of DNB (C_s) since it has only one H-bond for stabilization. Notably, other conformers with only one H-bond moiety also exist, but these will not be further discussed here.

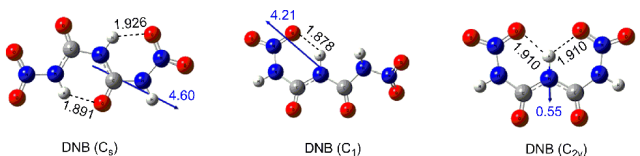


FIG. 3. Molecular structures of DNB conformers optimized at the M06-2X/aug-cc-pVTZ level. Intra-atomic distance for H-bonding is in Å. The dipole moment vector (blue) starts from the center of nuclear charge, unit in D. For DNB (C_{2v}), the dipole moment vector is amplified by a factor of 3.

As discussed above, these systems contain non-covalent contributions from electrostatic interactions as well as dispersion interactions, which can play an important role for both structures and energetics. It is known that the dipole moment can be used to measure non-uniform distributions of positive and negative charges on a molecule and its vector is dependent on the molecular configuration. The dipole moment for each of the biuret, MNB, and DNB conformers was calculated using the M06-2X/aug-cc-pVTZ optimized geometries as shown in Figures 1-3, where the dipole moment vector starts from the center of nuclear charge. It is seen that the dipole moment is 3.35 and 6.12 D, respectively, in biuret (*trans*) and biuret (*cis*). For MNB, the dipole moment is 3.21, 1.77, 8.02, and 3.61 D, respectively, in C_s , C_1 , *trans*-, and *cis*-conformers. For DNB, the dipole moment is 4.60, 4.21, and 0.55 D, respectively, in C_s , C_1 , and C_{2v} conformers. Biuret (*trans*), MNB (C_1), and DNB (C_{2v}) have significantly smaller dipole moments than their corresponding conformers, which is consistent with the fact that stable biuret, MNB, and DNB exist, respectively, in the *trans*, C_1 , and C_{2v} forms in the solid state as is observed experimentally.^{2,4} This reveals a simple way for evaluating reactivity of fuel conformers and suggests that, the planar MNB (*trans*), MNB (C_s), and MNB (*cis*), can be intermediates for a second NO₂ substitution to form DNB (C_s) and DNB (C_{2v}). It is seen that DNB (C_s) has a much larger dipole moment than DNB (C_{2v}), and its dipole moment vector points towards the H-atom which is not involved in hydrogen bonding; consequently, the DNB (C_s) can undergo a third NO₂ substitution. Yudin *et al.*³⁰ studied the nitration process of biuret and nitrobiuret in nitric acid and in mixed acids, and reported that the contents of the product mixture had an equilibrium nature to it, which depended on the acidity of the nitrating mixture and on the amount of nitric acid present. This indicates that the products of MNB and DNB materials¹ synthesized by nitration of biuret could be mixtures of several isomers.

B. PES of MNB thermal decomposition

Theoretical chemical kinetics on the thermal decomposition of MNB has not been reported previously. In this work, the PES for the thermal decomposition of MNB was investigated and the stationary point energies were calculated at the M06-2X/aug-cc-pVDZ, M06-2X/aug-cc-pVTZ, and RCCSD(T)/cc-pV ∞ Z/M06-2X/aug-cc-pVTZ levels of theory. The zero-point corrected energies (ZPE) at 0 K relative to the global energy minimum of MNB (C_s) are tabulated in Table I. Taking the RCCSD(T)/cc-pV ∞ Z results as a standard, it can be seen that the predictions at the M06-2X/aug-cc-pVDZ level of theory show remarkable agreement with those of the RCCSD(T)/cc-pV ∞ Z/M06-2X/aug-cc-pVTZ level of theory for the energy barrier heights, especially for the molecular elimination channels (within 0.1 kcal/mol). However, the discrepancy in the endothermicity is quite large, which can reach up to 3.7 kcal/mol. On the other hand, the M06-2X/aug-cc-pVTZ predictions show good agreement with that of the RCCSD(T)/cc-pV ∞ Z, for both the barrier heights and endothermicities. In particular, the discrepancy is on the order of 1.0 kcal/mol for the barrier heights and is within 1.8 kcal/mol for endothermicities, implying that the

TABLE I. Stationary point energies for MNB thermal decomposition.^a

Species	M06-2X/ aug-cc-pVDZ	M06-2X/ aug-cc-pVTZ	RCCSD(T)/cc-pV ∞ Z// M06-2X/aug-cc-pVTZ
MNB (C_s)	0.00	0.00	0.00
TS1	33.86	33.18	33.99
HBC-P1	18.50	20.51	19.43
IM1 + HNN(O)OH	29.42	26.85	27.08
TS2	34.58	33.73	34.66
HBC-P2	27.75	26.20	26.41
IM2 + HNCO	30.43	32.17	32.95
<i>trans</i> -biuret radical + NO ₂	51.41	51.34	52.75
MNB (C_1)	6.41	6.38	5.86
TS3	41.05	40.35	41.00
HBC-P3	34.23	32.65	32.47
IM3 + HNCO	40.33	38.46	38.77
TS4	53.77	54.71	53.71
NH ₂ C(O)NH ₂ + NO ₂ NCO	34.38	32.53	30.68
<i>iso-trans</i> -biuret radical + NO ₂	57.25	56.99	58.43
TS5	7.84	8.29	7.32

^aAll energies include zero-point corrections and are in kcal/mol relative to the global energy minimum of MNB (C_s).

M06-2X/aug-cc-pVTZ energies are good for larger analogous systems.

The PES for MNB thermal decomposition characterized at the RCCSD(T)/cc-pV ∞ Z//M06-2X/aug-cc-pVTZ level of theory is illustrated in Figure 4, in which reaction channels with energy barriers less than 53 kcal/mol are shown. The lowest energy isomer, MNB (C_s), has three major decomposition reaction pathways via: (1) HNN(O)OH molecular elimination, (2) HNCO molecular elimination, and (3) NO₂ elimination. Amongst these three channels, the NO₂ elimination path to produce isomeric *trans*-biuret radicals has a much higher energy barrier than those for the other

elimination channels, thus making it a less important process at MNB's ignition temperature and below. Hence here, only the molecular elimination channels R1 and R2 and their transition states (shown in Figure 9) are addressed in detail.

First, the thermal decomposition occurs by an intramolecular H-transfer from the central amino H-atom to the adjacent nitro O-atom via TS1 with an energy barrier of 33.99 kcal/mol. TS1 is a six-member-ring transition state with the cleaving N—H bond length of 1.577 Å, the forming O—H bond length of 1.033 Å, and the C—N bond elongated to 2.000 Å (the interatomic distances will be further discussed in Figure 9). Consequently, this channel eliminates HNN(O)OH and forms

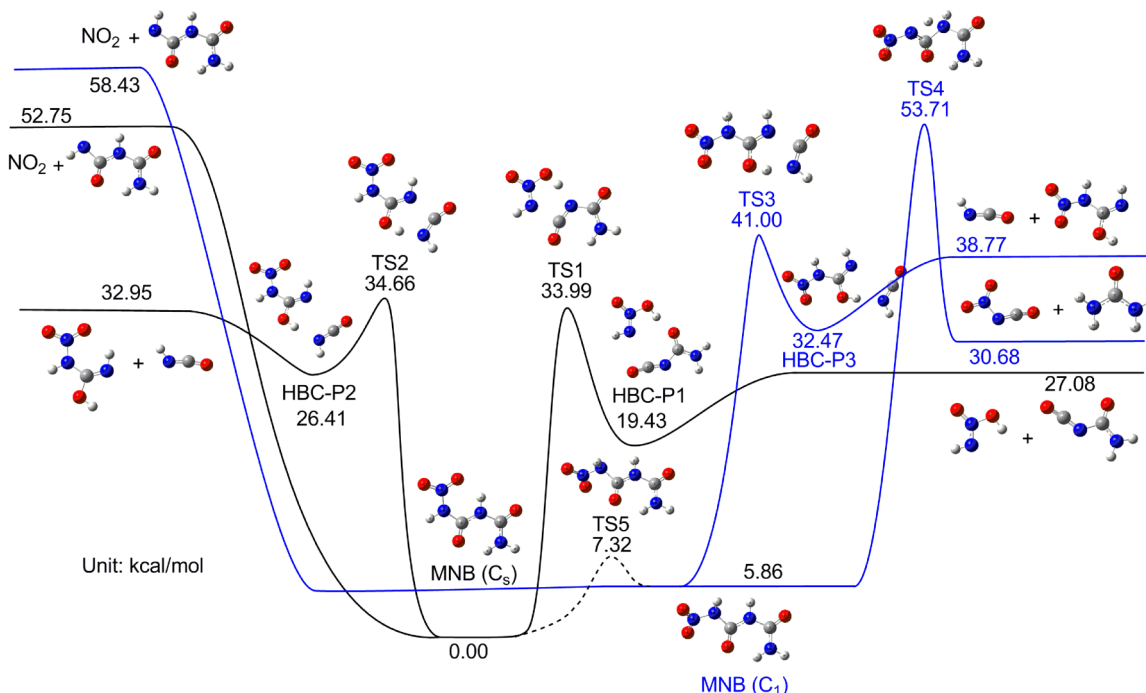


FIG. 4. The potential energy surface for the decomposition of MNB calculated at the RCCSD(T)/cc-pV ∞ Z//M06-2X/aug-cc-pVTZ level of theory.

the $\text{NH}_2\text{C}(\text{O})\text{NCO}$ intermediate (IM1) simultaneously. These two species were observed in the decomposition gas of MNB with their characteristic ion signals ($m/z = 62$ and $m/z = 86$).¹ This channel is endothermic by 27.08 kcal/mol and involves a H-bonded product-complex (HBC-P1) with energy of 7.65 kcal/mol below the exit channel. The HBC-P1 complex is characterized by hydrogen bonding between the hydroxyl H-atom and the carbonyl O-atom with an H-bond length of 1.685 Å, interatomic distance O—H···O of 2.668 Å, and angle $\angle \text{O}\cdots\text{H}\cdots\text{O}$ of 171.44°. Notably, the energized HNN(O)OH and IM1 intermediates undergo further decomposition. It was found that the primary reaction path for IM1 decomposition involves an intramolecular H-transfer to form two HNCO molecules via a four-member-ring transition state with an energy barrier of 48.20 kcal/mol. The decomposition mechanism of HNN(O)OH will be discussed later.

Second, MNB decomposition also occurs via an intramolecular H-transfer from the NH_2 group to the adjacent carbonyl oxygen via TS2 with an energy barrier of 34.66 kcal/mol. TS2 is also a six-member-ring transition state, which has the cleaving N—H bond length of 1.574 Å and the forming O—H bond length of 1.030 Å, with the C—N bond elongated to 2.036 Å. Consequently, this channel eliminates HNCO and co-forms the $\text{NO}_2\text{NHC}(\text{OH})\text{NH}$ intermediate (IM2) with reaction enthalpy of 32.95 kcal/mol. Another H-bonded product complex (HBC-P2) with energy of 6.54 kcal/mol below this exit channel was observed, which is characterized by hydrogen bonding between the hydroxyl H-atom and the N-atom of HNCO, with a H-bond length of 1.854 Å, interatomic distance O—H···N of 2.830 Å, and angle $\angle \text{N}\cdots\text{H}\cdots\text{O}$ of 171.50°. Both HBC-P1 and HBC-P2 have almost the same bond angle for hydrogen bonding, but the interatomic distance O—H···N in HBC-P2 is 0.162 Å longer than the distance O—H···O in HBC-P1. Consequently, hydrogen bonding in HBC-P2 is weaker and it is higher in energy than HBC-P1. Previous infrared data on evolved gases¹ indicate slow formation of HNCO between 160 °C and 186 °C. In addition, it was also reported that continued heating of MNB up to 350 °C showed only HNCO formation with no other decomposition gas products. Klapötke *et al.*¹ interpreted the observed HNCO formation by the secondary decomposition through $\text{NH}_2\text{C}(\text{O})\text{NCO}$ (IM1) generated from channel R1. As we indicated above, the decomposition of IM1 to form HNCO has an energy barrier of 48.20 kcal/mol. Here instead, we have found a primary HNCO product formation path via MNB (C_s) involving direct molecular elimination through TS2. This primary HNCO product formation path also applies to the decomposition of the stable conformer MNB (C_1) via TS3.

As discussed above, stable MNB exists in the asymmetric C_1 form in the solid state, with 5.86 kcal/mol higher energy than that for the C_s form. Three reaction pathways for elimination of HNCO, $\text{NH}_2\text{C}(\text{O})\text{NH}_2$ (urea), and NO_2 from MNB (C_1) are shown in Figure 4 as blue curves. It was found that the elimination channels for HNCO and NO_2 in MNB (C_1) have similar barrier heights, endothermicities, and product-complex energies as those in MNB (C_s). While elimination of urea from MNB (C_1) is different, it occurs by an intramolecular H-transfer from nitramine H-atom to the adjacent amino N-

atom via TS4 with an energy barrier of 53.71 kcal/mol. TS4 is a 4-member-ring transition state, with the cleaving N—H bond length of 1.329 Å, the forming N—H bond length of 1.280 Å, and the C—N bond elongated from 1.368 to 1.533 Å. This channel produces NO_2NCO and urea and is endothermic by 24.82 kcal/mol. Urea was also observed in the MNB pyrolysis experiment with an ion signal at $m/z = 60$ and was reported to be the precursor for biuret, triuret, tetrauret, and cyanuric acid formation.¹ However, urea formation in the previous MNB pyrolysis experiment was interpreted to be from the gas phase reaction of NH_3 with HNCO , where NH_3 is from the reaction of HNCO with H_2O , and H_2O is from the decomposition of NH_2NO_2 .¹ We note that urea might be formed from these sequential reactions; however, we find direct decomposition from MNB (C_1) via TS4 to be the primary reaction path in the present study.

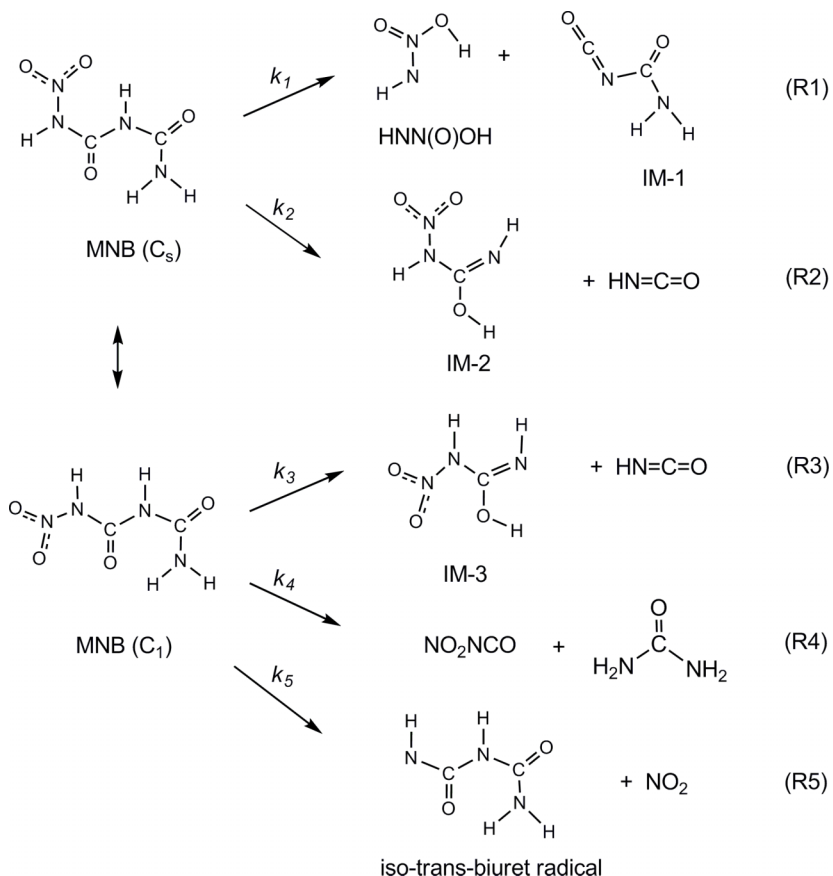
C. Ab initio kinetics of MNB thermal decomposition

Based on the above PES, the primary reaction pathways for MNB thermal decomposition are depicted in reaction Scheme 1. The rate coefficients at the high-pressure limit for reactions R1-R4 were determined explicitly by micro-canonical transition state theory at the E , J resolved level. R5 involves the N—N bond fission of MNB (C_1) without any reverse energy barrier. For this channel, the rate coefficient was determined with reaction enthalpy of 52.57 kcal/mol determined herein, and the reverse rate coefficient of $8.69 \times 10^{-12} \text{ T}^{-0.033} \exp(-315/\text{T}) \text{ cm}^{-3} \text{ molecule}^{-1} \text{ s}^{-1}$ adopted from the reaction $\text{NH}_2 + \text{NO}_2 \rightarrow \text{NH}_2\text{NO}_2$.³² The obtained rate coefficients for R1-R5 were fitted over 300-2500 K by the following modified Arrhenius expressions in units of s^{-1} :

$$\begin{aligned} k_{1,\infty} &= 1.32 \times 10^{13} \text{ T}^{0.131} \exp(-17474.7/\text{T}), \\ k_{2,\infty} &= 1.05 \times 10^{13} \text{ T}^{0.112} \exp(-17692.1/\text{T}), \\ k_{3,\infty} &= 1.15 \times 10^{14} \text{ T}^{-0.117} \exp(-18011.4/\text{T}), \\ k_{4,\infty} &= 1.26 \times 10^4 \text{ T}^{2.539} \exp(-21375.5/\text{T}), \\ k_{5,\infty} &= 2.07 \times 10^{23} \text{ T}^{-2.002} \exp(-27714.8/\text{T}). \end{aligned}$$

As shown in Figure 5, at the high-pressure limit, k_1 , k_2 , and k_3 are comparable at all temperatures. Furthermore, the rate coefficients k_∞ for elimination of HNCO are similar for C_1 and C_s conformers. Below 1200 K, HNCO and HNN(O)OH elimination channels are dominant for both isomers, which is consistent with previous experimental observations.¹ Above 1200 K, NO_2 elimination channel becomes dominant. The elimination of urea is slow but it becomes significant at temperatures above 1000 K.

As shown in Figure 4, conversion of isolated MNB (C_1) into MNB (C_s) can be facilitated by rotation of the C—NHNO₂ bond via TS5. Since the energy barrier for this rotation is only 1.46 kcal/mol, equilibration between the conformers is expected to be fast, and the initial decomposition of MNB can be simplified into a single-well and multiple-channel reaction system for kinetics analysis. For evaluating the pressure dependence of unimolecular decomposition rate, the collisional energy transfer probability was approximated by the $\Delta E_{\text{down}} = 200 \times (\text{T}/300)^{0.85} \text{ cm}^{-1}$ model for the average downward energy transfer.³¹ The theoretical rate coefficients at



SCHEME 1. Primary reaction pathways in MNB thermal decomposition.

a pressure of 1 atm (N_2) for MNB (C_1) thermal decomposition channels are presented in Figure 6. Compared to the rate coefficients at the high-pressure limit (shown in Figure 5), these decomposition channels have strong pressure dependences. Furthermore, HNN(O)OH and HNCO elimination channels are competitive and dominant below 2500 K, and elimination of NO_2 becomes competitive only above 2500 K. From this, we conclude that HNN(O)OH (from R1) and HNCO (from R2 and R3) are the primary products for MNB decomposition at ignition temperatures.

D. Ab initio kinetics of DNB thermal decomposition

As discussed in Sec. III B, the energy barrier heights and endothermicities in the decomposition of the MNB system predicted by M06-2X/aug-cc-pVTZ calculations show remarkable agreement with those predicted from RCCSD(T)/cc-pV ∞ Z//M06-2X/aug-cc-pVTZ calculations. Consequently, the saddle point energies on the PES for the decomposition of the analogous DNB system were determined by M06-2X/aug-cc-pVDZ and M06-2X/aug-cc-pVTZ levels of theory. The saddle point energies on the PES for the DNB decomposition system listed in Table II are relative to the global energy minimum for DNB (C_s). Specifically, for the M06-2X/aug-cc-pVDZ energies, the zero-point corrections were determined at the same level of theory. For the M06-2X/aug-cc-pVTZ energies, the zero-point corrections were determined at the same level of theory except for the transition states and H-bonded product-complexes, which were determined at the M06-2X/aug-cc-pVDZ level of

theory. From Table II, it can be seen that the energy barrier heights predicted from these two levels of calculation show excellent agreement, but discrepancy reaches to 2.1 kcal/mol for reaction endothermicities. Consequently, the M06-2X/aug-cc-pVTZ energies were used for carrying out the kinetics analysis for DNB decomposition.

The PES for the DNB thermal decomposition system is shown in Figure 7. The DNB (C_s) conformer has four reaction pathways, which are similar to that for MNB (C_s). First, thermal decomposition occurs by an intramolecular H-transfer from central amino H-atom to the adjacent nitro O-atom via TS6 with an energy barrier of 33.77 kcal/mol, producing two intermediates (HNN(O)OH + $NO_2NHC(O)NCO$) with energy of 26.79 kcal/mol via a H-bonded complex, HBC-P6 with energy of 6.49 kcal/mol below the exit asymptote. Second, the decomposition also occurs by another intramolecular H-transfer, from central amino group to the adjacent nitro-oxygen via TS7 (also shown in Figure 9) with an energy barrier of 31.21 kcal/mol, to produce the (IM2 + NO_2NCO) species with energy of 36.91 kcal/mol. In this channel, TS7 is 5.70 kcal/mol lower in energy compared to its exit asymptote. Compared to the analogous channel (R2) for HNCO elimination in MNB, the energy barrier for TS7 is 3.45 kcal/mol lower, which can be ascribed to the late transition state TS7 due to the electron withdrawing effect from the NO_2 group in NO_2NCO . Furthermore, DNB (C_s) also undergoes N—N bond fissions with energy barriers of 49.79 and 51.09 kcal/mol to eliminate each of the terminal NO_2 groups to form two radical intermediates, *trans*-MNB radical and C_1 -MNB radical, respectively. We note that the

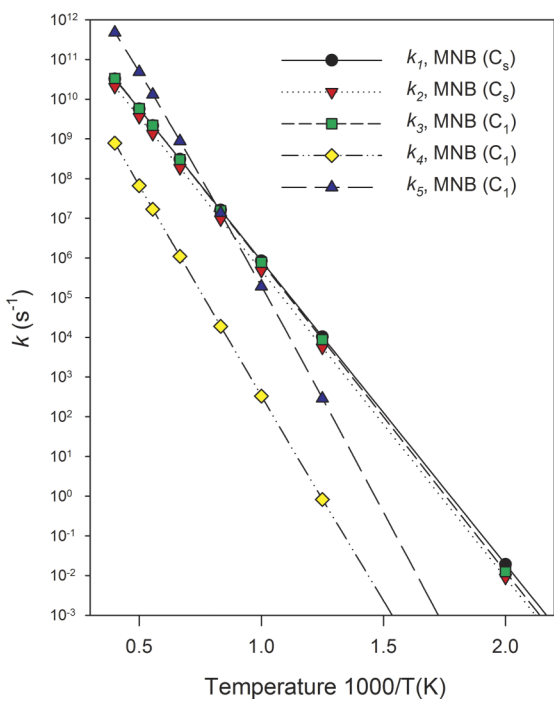


FIG. 5. Rate coefficients at the high-pressure limit for MNB (C_{2v}) and MNB (C_1) primary thermal decomposition channels.

parent molecules of these two radicals are *trans*- and C_{2v} -forms of MNB, as shown in Figure 2.

Figure 7 also shows two decomposition channels for the DNB (C_{2v}) conformer (blue lines): HNN(O)OH molecular elimination and N—N bond fission. The molecular elimination channel proceeds via an intramolecular H-transfer from central amino H-atom to the adjacent nitro O-atom

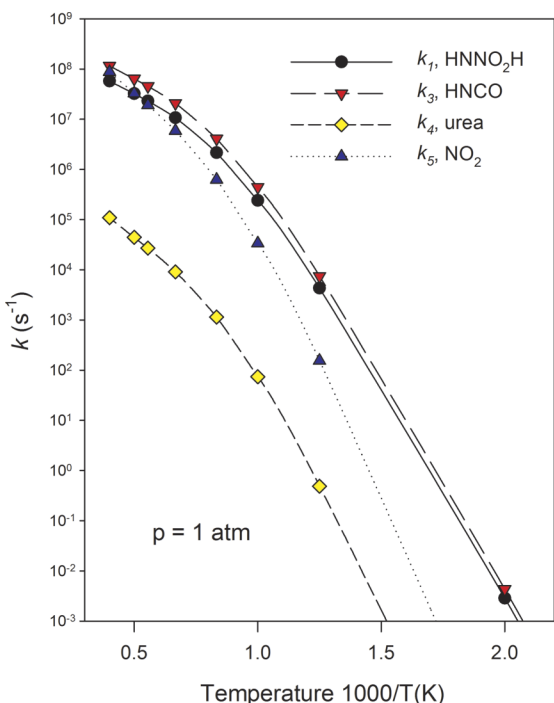


FIG. 6. Rate coefficients at pressure of 1 atm for MNB (C_{2v}) and MNB (C_1) primary thermal decomposition channels.

through TS8 (shown in Figure 9) to yield HNN(O)OH and iso- $\text{NO}_2\text{NHC(O)NCO}$ intermediates with an energy barrier of 28.61 kcal/mol. Due to the C_{2v} symmetry, the N—N bond fission only produces *cis*-MNB radical + NO_2 , which has an energy asymptote of 52.84 kcal/mol. The DNB (C_{2v}) to DNB (C_{2v}) transformation can be achieved by a two-step rotation mechanism⁶ as illustrated in Figure 7, rather than by a single rotation step.²⁹ It can proceed by rotation of the C—NHNO₂ bond via TS9 to the DNB (C_1) conformer and then by rotation of the N—CONHNO₂ bond via TS10. However, we note that fast equilibrium between the two DNB conformers is not likely due to the need for multiple rotations, which require overcoming higher barriers and larger entropy changes compared to the case present in MNB. Instead, direct decomposition to release HNN(O)OH via the planar transition state, TS8 is kinetically more favorable. Consequently, the primary reaction pathways for DNB thermal decomposition can be described by reaction Scheme 2. The corresponding rate coefficient at the high-pressure limit was then determined for each individual channel. The theoretical rate coefficients as a function of temperature in the range 300–2500 K were fitted to the modified Arrhenius expressions in units of s^{-1} , which are given below and illustrated in Figure 8,

$$\begin{aligned}k_{6,\infty} &= 3.22 \times 10^{14} T^{-0.289} \exp(-17567.7/T), \\k_{7,\infty} &= 8.49 \times 10^{16} T^{-0.882} \exp(-17048.6/T), \\k_{8,\infty} &= 9.72 \times 10^{13} T^{-0.248} \exp(-14228.7/T), \\k_{9,\infty} &= 9.96 \times 10^{23} T^{-2.205} \exp(-27286.3/T).\end{aligned}$$

It was found that $k_{6,\infty}$ for elimination of HNN(O)OH is consistent with $k_{1,\infty}$ and $k_{2,\infty}$ because of the similarity in the barrier heights and nature of the six-member-ring transition states. In addition, $k_{9,\infty}$ is also consistent with $k_{5,\infty}$ for NO_2 elimination because of the similar barrier heights and the adoption of the same reverse reaction rate coefficient.³² In Figure 8, it is seen that $k_{8,\infty}$ for the elimination channel for HNN(O)OH from DNB (C_{2v}) is dominant below 1500 K, and $k_{9,\infty}$ for the NO_2 elimination channel from DNB (C_{2v}) is dominant above 1500 K. The coefficients $k_{6,\infty}$ and $k_{7,\infty}$ for the HNN(O)OH and NO_2NCO elimination channels from DNB (C_{2v}) are significantly smaller than $k_{8,\infty}$ below 1000 K. $k_{7,\infty}$ becomes comparable with $k_{8,\infty}$ above 1000 K, but it is smaller than $k_{9,\infty}$ at temperatures above 1000 K. Therefore, DNB (C_{2v}) has the largest rate coefficients for its unimolecular decomposition at all temperatures. Figure 8 also shows $k_{8,\infty}$ and $k_{9,\infty}$ from the B3LYP/6-31+G** calculations and RRKM results of Liu *et al.*⁵ in the range 750–2000 K. It is seen that their $k_{8,\infty}$ is in agreement with that of this study at temperatures above 1500 K, but it is significantly smaller below ~1500 K. Their $k_{9,\infty}$ is also significantly smaller than that of the present study. At 1500 and 2000 K, we found the high-pressure limit rate coefficients to be, respectively, a factor of 48 and 13 smaller than the present values. Such a large discrepancy could be ascribed to the fact that for this N— NO_2 bond fission transition state, they estimated the reaction enthalpy to be ~40 kcal/mol and also they empirically estimated the vibrational frequencies from those of DNB, *cis*-MNB radical, and NO_2 . It is also noted that their reaction

TABLE II. Stationary point energies for DNB thermal decomposition.^a

Species	M06-2X/aug-cc-pVDZ	M06-2X/aug-cc-pVTZ
DNB (C_s)	0.00	0.00
TS6	34.17	33.77
HBC-P6	21.58	20.30
HNN(O)OH + NO ₂ NHC(O)NCO	28.68	26.79
TS7	31.72	31.21
HBC-P7	30.70	29.98
IM2 + NO ₂ NCO	34.79	36.91
C_1 -MNB radical + NO ₂	50.20	49.79
<i>trans</i> -MNB radical + NO ₂	50.89	51.09
DNB (C_{2v})	1.16	1.22
TS8	28.64	28.61
HBC-P8	22.35	21.70
HNN(O)OH + iso-NO ₂ NHC(O)NCO	29.08	27.26
<i>cis</i> -MNB radical + NO ₂	52.54	52.84
DNB (C_1)	7.45	7.82
TS9	9.42	10.32
TS10	10.79	11.20

^aAll energies include zero-point corrections and are in kcal/mol relative to the global energy minimum of DNB (C_s).

enthalpy is ~10 kcal/mol lower than the typical value of N—NO₂ bond dissociation energy.

E. Thermal stability of DNB compared with MNB

Klapötke *et al.*¹ reported that DNB is unstable and heat sensitive, and the energies of activation for decomposition of MNB and DNB were estimated from heat release vs. reaction time to be 51 and 35 kcal/mol, respectively, for which they assumed the rate coefficients followed the Arrhenius rate law and that the decomposition could be considered to occur via a single step. Nevertheless, their work showed DNB is more unstable and heat sensitive compared with MNB.

Our kinetic analyses show that the rate coefficients for the primary channels for DNB (C_{2v}) decomposition are larger than that for MNB, which is mainly due to the correspondingly lower barrier heights. In particular, (1) for the intramolecular elimination of HNN(O)OH channel, the energy barrier via TS1 or TS3 is 34–35 kcal/mol for the C_s or C_1 conformer of MNB, and the energy barrier via TS8 is 27.39 kcal/mol for the DNB (C_{2v}) conformer, and (2) for the intramolecular elimination of HNCO or NO₂NCO channel, the energy barrier via TS2 for MNB is 34.66 kcal/mol, and 31.21 kcal/mol via TS7 for DNB (C_{2v}). It was found that the different barrier heights for the same type of reaction can be ascribed to the strength of the H-bonding and the intramolecular distances in the respective

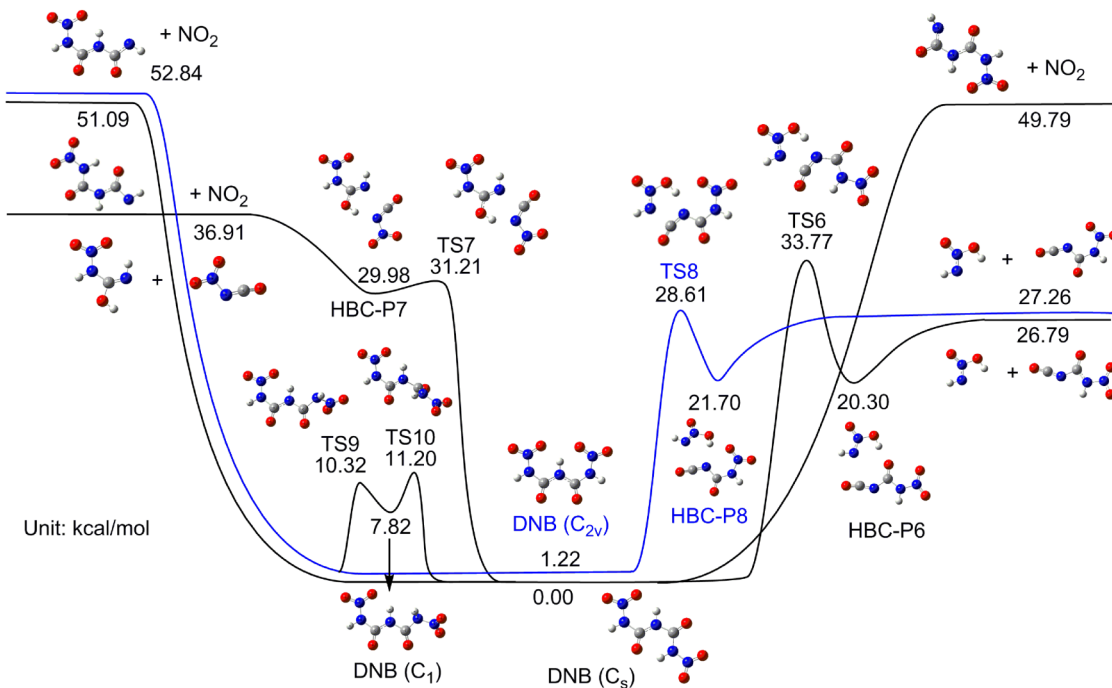
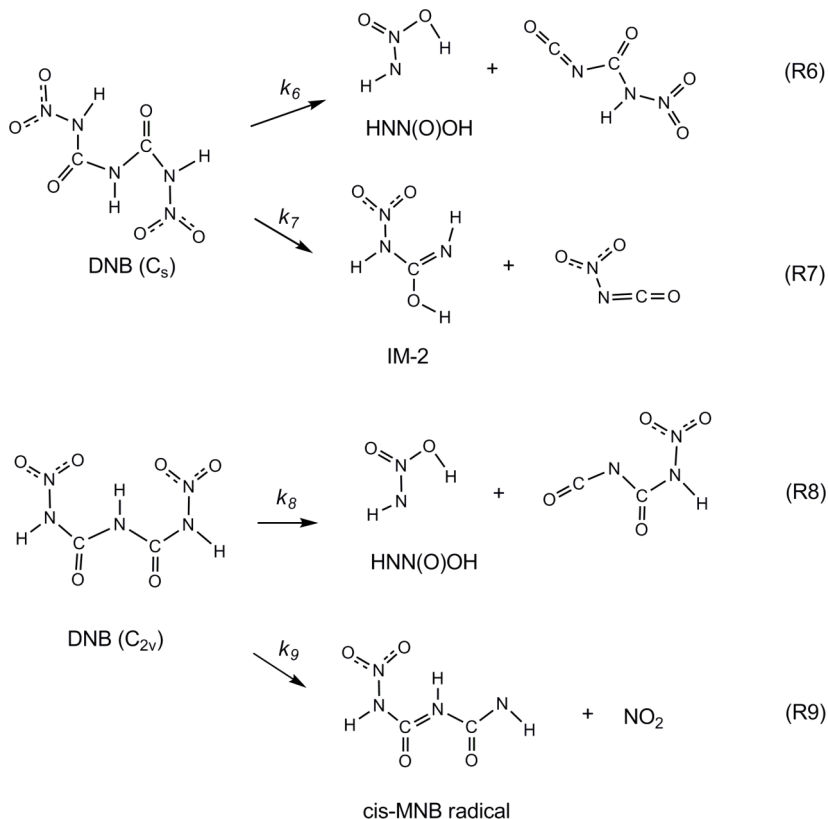


FIG. 7. The potential energy surface for the thermal decomposition of DNB calculated at the M06-2X/aug-cc-pVTZ level of theory.



SCHEME 2. Primary reaction pathways in DNB thermal decomposition.

transition states. Figure 9 shows the interatomic distances in two analogous sets of transition states, TS1 vs. TS8, and TS2 vs. TS7. For the intramolecular elimination of HNN(O)OH, the interatomic distance between the hydroxyl H-atom and the adjacent carbonyl O-atom in TS1 is 3.012 Å. While the corresponding interatomic distance is 2.118 Å in the analogous transition state TS8, which in this case is short enough to form an intramolecular hydrogen bond. Consequently, TS8 is stabilized by an extra H-bonding and therefore the energy barrier is decreased by 6.60 kcal/mol compared to TS1. For the molecular elimination of HNCO from MNB, the transition state TS2 is late, as indicated by the cleaving N—H and C—N bond lengths and the forming O—H bond length. However, the molecular elimination of NO₂NCO from DNB via TS7 is even later due to the strong electron withdrawing effect of NO₂ in the NO₂NCO fragment, where the cleaving N—H and C—N bond lengths are 1.820 Å and 2.243 Å, respectively. This causes the energy barrier for NO₂NCO elimination in DNB to be 3.45 kcal/mol lower than that for HNCO elimination in MNB.

For comparison proposes, the pressure dependence of DNB decomposition rate coefficients were evaluated with the same collisional energy transfer probability model used in the MNB decomposition. The resulting rate coefficients at a pressure of 1 atm (N₂) for DNB (C_{2v}) thermal decomposition channels are shown in Figure 10. Compared with pressure-dependent rate coefficients for MNB decomposition shown in Figure 6, it can be seen that k_8 for the elimination of HNN(O)OH from DNB is much larger than k_1 for MNB below 800 K. Furthermore, k_8 is 2 orders of magnitude larger than k_9 at 500 K. Since intramolecular elimination of HNN(O)OH

is the primary process for both MNB and DNB thermal decomposition below 1200 K, the above comparison provides a quantitative interpretation for the thermal instability of DNB compared to MNB.

F. Thermal decomposition of HNN(O)OH intermediate

As an intermediate formed from the primary dissociation channel of both MNB and DNB, HNN(O)OH can undergo further decomposition. The thermal decomposition of HNN(O)OH has not been reported in the literature. In this work, the PES for HNN(O)OH thermal decomposition is shown in Figure 11, which was characterized by several different *ab initio* quantum chemical approaches as discussed in Sec. II A. It was found that HNN(O)OH has several conformers with nearly identical energies, and it decomposes via multiple wells and multiple channels. To differentiate the various HNN(O)OH isomers, the conformer that directly dissociated from MNB or DNB was named *trans*-HNN(O)OH (*trans*), as it has a geometry in which the OH group is *trans* to the NH group along the N—N bond and *trans* to the N=O group along the N—OH bond. With this geometry, an internal rotation of OH along the N—O bond results in the *trans*-HNN(O)OH (*cis*) conformer, which has the OH group *cis* to the N=O group. Subsequently, another internal rotation of NH along the N—N bond forms the *cis*-HNN(O)OH (*cis*) conformer, which has the NH group *cis* to the OH group.

It was found that the *trans*-HNN(O)OH (*trans*) conformer dissociates via the following three reaction pathways: (1) a direct N—OH bond fission to produce OH + *cis*-HNNO, (2)

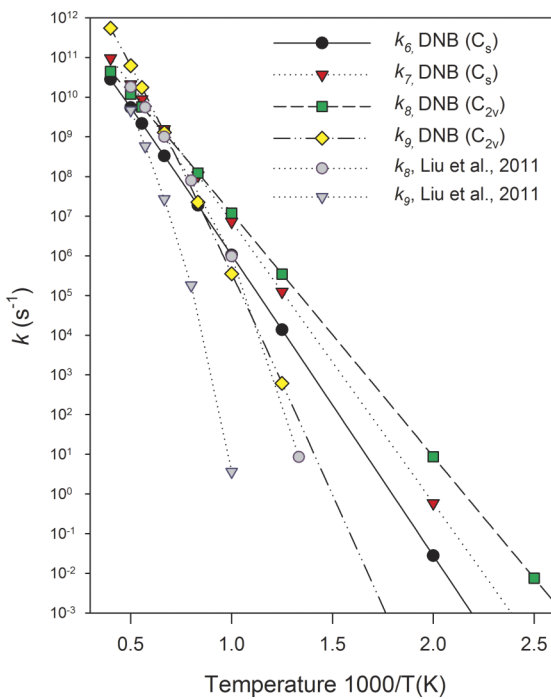


FIG. 8. Rate coefficients at the high-pressure limit for DNB (C_3) and DNB (C_{2v}) primary thermal decomposition channels.

isomerization to the *cis*-HNN(O)OH (*cis*) conformer followed by decomposition to generate $N_2O + H_2O$ and $OH + trans$ -HNNO, and (3) isomerization to the nitramine followed by decomposition to yield $NH_2 + NO_2$. Specifically, for the direct N—OH bond fission, the process is endothermic by 52.73 kcal/mol. A relaxed N—OH bond scan of *trans*-HNN(O)OH (*trans*) at the CASPT2(4e, 3o) level of theory, with state-averaged active space consisting of two degenerate *p* orbitals for the OH and *p* orbitals for N-atoms, shows that the bond fission occurs with a loose transition state geometry with energy of 48.44 kcal/mol and forms a H-bonded complex with energy of 4.67 kcal/mol lower than its exit asymptote. For simplification, this bond fission potential was treated by a two-transition-state model¹⁹ with a coefficient of 1.68

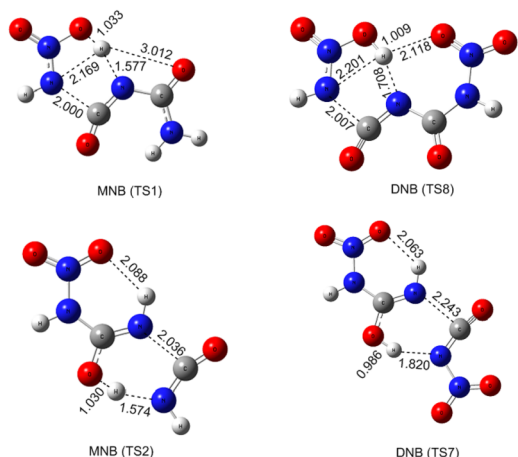


FIG. 9. Geometries of TS1 and TS2 optimized at the M06-2X/aug-cc-pVTZ level of theory and geometries of TS7 and TS8 at the M06-2X/aug-cc-pVQZ level of theory.

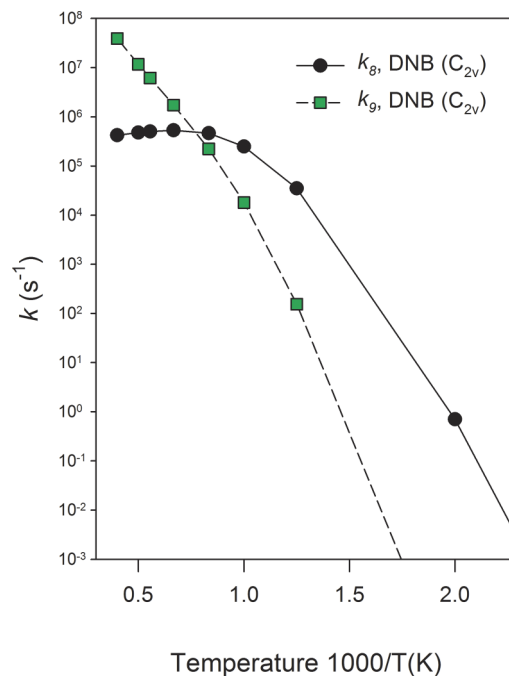


FIG. 10. Rate coefficients at a pressure of 1 atm for DNB (C_{2v}) primary thermal decomposition channels.

$\times 10^5 \text{ Å}^6 \text{ cm}^{-1}$ for the long-range isotropic potential, and the high-pressure limit rate coefficient for decomposition of *trans*-HNN(O)OH (*trans*) to $OH + cis$ -HNNO was determined to be $3.03 \times 10^{18} T^{-0.856} \exp(-27020.0/T) \text{ s}^{-1}$ in the temperature range 500–2500 K. This rate coefficient is in good agreement with that derived from its reverse reaction coefficient by Klippenstein *et al.*³²

The transformation of *trans*-HNN(O)OH (*trans*) to *cis*-HNN(O)OH (*cis*) can occur by internal rotation followed by isomerization. In particular, the transformation may occur via the rotation of the N—OH bond with energy barrier of 5.59 kcal/mol to form *trans*-HNN(O)OH (*cis*) and then another rotation of the N—NH bond with energy barrier of 31.45 kcal/mol. In the *trans*-HNN(O)OH (*cis*), a hydroxyl H-atom transfer to the nitric oxygen can also occur to form *cis*-HNN(O)OH (*cis*) with energy barrier of 26.25 kcal/mol. In the RRKM master equation simulations, the sums of the partition functions for the two latter transition states were evaluated for the rate calculations. Furthermore, it was found that the rotation of the aminylene H-atom in *trans*-HNN(O)OH (*trans*) conformer repels the hydroxyl H-atom leading to the formation of *cis*-HNN(O)OH (*cis*) with energy barrier of 30.11 kcal/mol. The *cis*-HNN(O)OH (*cis*) conformer undergoes endothermic N—OH bond fission to form $OH + trans$ -HNNO or exothermic decomposition to $N_2O + H_2O$. Notably, the decomposition to $N_2O + H_2O$ releases 50.51 kcal/mol of enthalpy, which can promote the ignition process in MNB and DNB.

Direct isomerization of *trans*-HNN(O)OH (*trans*) via a four-member-ring transition state to form the nitramide which then dissociates to $NH_2 + NO_2$ is also possible. The PES for the reverse reaction, $NH_2 + NO_2$, has been previously studied both theoretically and experimentally.^{32–35} The stationary point energies on the PES for *trans*-HNN(O)OH (*trans*) decomposi-

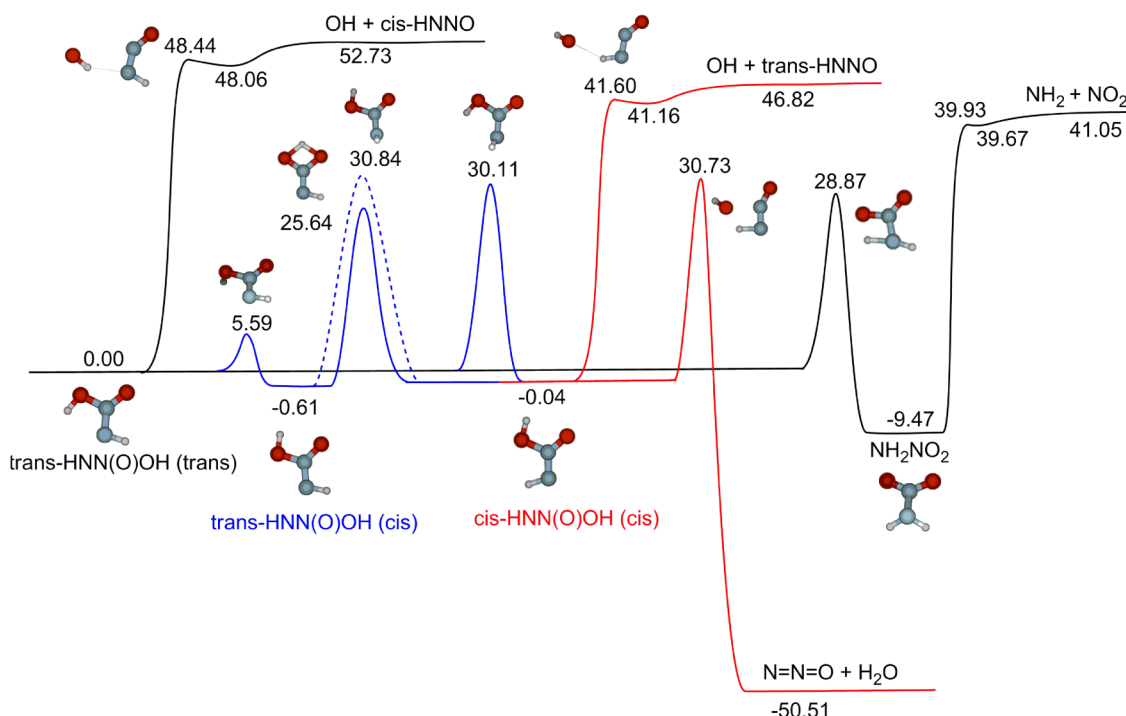


FIG. 11. Potential energy surface for $\text{HNN}(\text{O})\text{OH}$ thermal decomposition calculated by several *ab initio* methods (see text). Energies are zero-point corrected and relative to *trans*- $\text{HNN}(\text{O})\text{OH}$ (*trans*) at 0 K.

tion, relative to the $\text{NO}_2 + \text{NH}_2$ energy asymptote, are listed in Table III. These energies are compared with recently published data by Klippenstein *et al.*,³² where the energies were determined by the spin restricted quadratic configuration interaction, RQCISD(T)/CBS(QZ, 5Z)//B3LYP/6-311++G(d,p) method and HL estimates. Specifically, the HL energies were obtained through the combination of UCCSD(T)/cc-pVTZ ro-vibrational analysis with UCCSD(T)/CBS(aug-cc-pVQZ, aug-cc-pV5Z) energies, and several additional higher order corrections and B3LYP/6-311++G(d,p) anharmonic ZPE corrections. From Table III, it is seen that the stationary point energies from this work are in excellent agreement with those of Klippenstein *et al.*,³² with discrepancy between the different

methods within ~ 1 kcal/mol. It has been reported that the RQCISD(T)/CBS method has uncertainties of ~ 1 kcal/mol, and the uncertainties for the HL method are on the order of ~ 0.3 kcal/mol or less when multi-reference effects are not substantial.³² Notably, we provide here an alternate approach for obtaining high-accuracy geometries, vibrational frequencies, and enthalpy data for this reaction system.

Choosing the reaction of $\text{OH} + \text{cis}$ -HNNO as the entrance channel, the pressure-dependent rate coefficients for the decomposition of *trans*- $\text{HNN}(\text{O})\text{OH}$ (*trans*) were determined by RRKM theory with multi-well master equation simulations at the E, J resolved level. The collisional energy transfer probability was approximated using ΔE_{down}

TABLE III. Stationary point energies for *trans*- $\text{HNN}(\text{O})\text{OH}$ (*trans*) thermal decomposition.^a

Species	RQCISD(T)/CBS ^b	UCCSD(T)/CBS ^b	RCCSD(T)/CBS
$\text{NH}_2 + \text{NO}_2$	0.00	0.00	0.00
H_2NNO_2	-50.40	-49.90	-50.52
<i>trans</i> - $\text{HNN}(\text{O})\text{OH}$ (<i>cis</i>)	-41.47	-41.04	-41.66
<i>cis</i> - $\text{HNN}(\text{O})\text{OH}$ (<i>cis</i>)	-41.30	-40.78	-41.09
$\text{H}_2\text{O} + \text{NNO}$	-90.96	-90.55	-91.56
<i>trans</i> -HNNO + OH	5.46	4.93	5.77
<i>cis</i> -HNNO + OH	11.33	11.20	11.68
$\text{H}_2\text{NNO}_2 \leftrightarrow \text{trans}$ - $\text{HNN}(\text{O})\text{OH}$ (<i>trans</i>)	-12.58	-11.62	-12.18
<i>trans</i> - $\text{HNN}(\text{O})\text{OH}$ (<i>cis</i>) \leftrightarrow <i>cis</i> - $\text{HNN}(\text{O})\text{OH}$ (<i>cis</i>); isomerization	-15.68	-14.67	-15.41
<i>trans</i> - $\text{HNN}(\text{O})\text{OH}$ (<i>cis</i>) \leftrightarrow <i>cis</i> - $\text{HNN}(\text{O})\text{OH}$ (<i>cis</i>); torsion	-10.87	-9.96	-10.21
<i>cis</i> - $\text{HNN}(\text{O})\text{OH}$ (<i>cis</i>) $\leftrightarrow \text{H}_2\text{O} + \text{N}_2\text{O}$	-10.81	-10.26	-10.32
<i>trans</i> - $\text{HNN}(\text{O})\text{OH}$ (<i>trans</i>)			-41.05
<i>trans</i> - $\text{HNN}(\text{O})\text{OH}$ (<i>trans</i>) \leftrightarrow <i>cis</i> - $\text{HNN}(\text{O})\text{OH}$ (<i>cis</i>)			-10.94
<i>trans</i> - $\text{HNN}(\text{O})\text{OH}$ (<i>trans</i>) $\leftrightarrow \text{trans}$ - $\text{HNN}(\text{O})\text{OH}$ (<i>cis</i>)			-35.46

^aAll energies include zero-point corrections and are in kcal/mol relative to the $\text{NH}_2 + \text{NO}_2$ energy asymptote.

^bFrom Ref. 32.

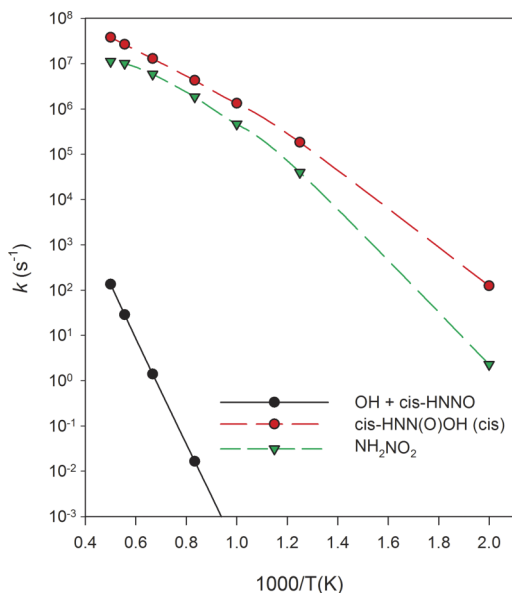


FIG. 12. Rate coefficients for *trans*-HNN(O)OH (*trans*) decomposition channels at a pressure of 1 atm.

$= 125 \times (T/300)^{0.85} \text{ cm}^{-1}$ as the average downward energy transfer. As shown in Figure 12, at a pressure of 1 atm, isomerization to *cis*-HNN(O)OH (*cis*) is the most dominant process, while isomerization to NH₂NO₂ is competitive, and N—OH bond fission to OH + *cis*-HNNO is relatively slow. Consequently, the subsequent decomposition reactions of *cis*-HNN(O)OH (*cis*) and NH₂NO₂ are important reactions in *trans*-HNN(O)OH (*trans*) decomposition. Figure 13 shows the rate coefficients for *cis*-HNN(O)OH (*cis*) decomposition at a pressure of 1 atm. It is seen that the formation of N₂O + H₂O is the predominant process. As a result, the thermal decomposition of *trans*-HNN(O)OH (*trans*) intermediate mainly produces the thermodynamically stable N₂O + H₂O products, which is consistent with previous experimental observations.¹

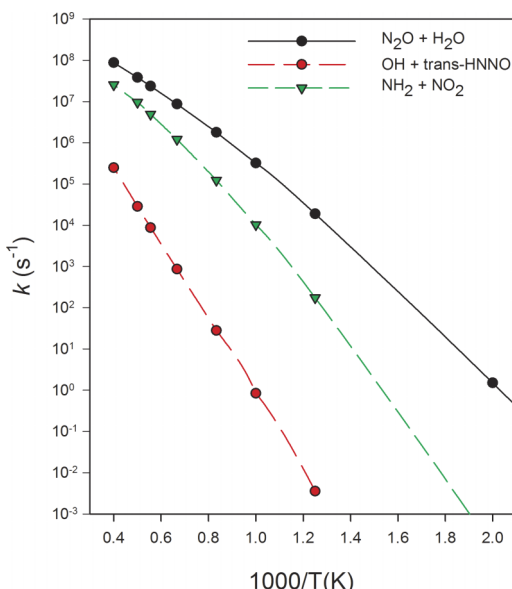


FIG. 13. Rate coefficients for *cis*-HNN(O)OH (*cis*) decomposition channels at a pressure of 1 atm.

IV. CONCLUSIONS

For the first time, we report a comprehensive study on the thermal decomposition mechanisms for mononitrobiuret and 1,5-dinitrobiuret through the application of advanced quantum chemistry and *ab initio* kinetics theories. Both MNB and DNB are stabilized via 6-member-ring moieties involving intramolecular H-bonding resulting from electrostatic as well as polarization and dispersion interactions. Furthermore, it was found that the stable molecules in the solid state have the smallest dipole moment amongst all the conformers in the nitrobiuret series of compounds, thus revealing a simple way for evaluating reactivity of fuel conformers.

The PESs for thermal decomposition of MNB and DNB were characterized at the M06-2X/aug-cc-pVTZ and RCCSD(T)/cc-pV ∞ Z//M06-2X/aug-cc-pVTZ level of theory. In particular, the values of the energy barriers and endothermicities at the M06-2X/aug-cc-pVTZ level of theory show remarkable agreement with the values obtained from the RCCSD(T)/cc-pV ∞ Z//M06-2X/aug-cc-pVTZ computations, implying that the former level of theory could be applicable to larger analogous systems.

It was found that the thermal decomposition of MNB is initiated by the elimination of HNCO and HNN(O)OH intermediate, the latter is also released from a primary decomposition channel in DNB (C_{2v}). The energy barrier for HNN(O)OH elimination in DNB is 6.60 kcal/mol lower than that in MNB due to an extra hydrogen bond in the transition state for the former, which results in DNB being less stable than MNB. Furthermore, the HNN(O)OH intermediate subsequently decomposes via multiple wells and multiple channels. The RRKM/multi-well master equation simulations revealed that decomposition to thermodynamically stable N₂O + H₂O products via isomerization is the primary channel during HNN(O)OH decomposition. The rate coefficients for the primary decomposition channels were quantified as functions of temperature and pressure. The present reaction kinetics study on MNB and DNB thermal decomposition provides theoretical interpretations of the experimentally observed decomposition products and the thermal instability of DNB. It also provides a fundamental understanding of the molecular structures of nitrobiurets and key reactions leading to ignition in these nitro-substituted systems. Such information is essential in the design and manipulation of molecular systems for the development of new energetic materials for advanced propulsion applications.

ACKNOWLEDGMENTS

We acknowledge Dr. Stephen J. Klippenstein at Argonne National Laboratory for his technical support on the NH₂ + NO₂ reaction system. H. Sun acknowledges the National Research Council for the Senior Research Associateship Award at the Air Force Research Laboratory, Edwards AFB under Contract No. FA9550-12-d-0001. This research was performed using the following resources: (1) The National Energy Research Scientific Computing Center, which is supported by the Office of Science of the U.S. Department of Energy under Contract No. DE-AC02-05CH11231; (2) The

William R. Wiley Environmental Molecular Sciences Laboratory (EMSL), which is sponsored by the U.S. Department of Energy's Office of Biological and Environmental Research, located at Pacific Northwest National Laboratory (PNNL); and (3) The DoD High Performance Computing Modernization Program at the Air Force Research Laboratory, Army Research Laboratory, Engineer Research and Development Center, and Navy Department of Defense Supercomputing Resource Centers (DSRCs).

- ¹J. Geith, G. Holl, T. M. Klapötke, and J. J. Weigand, *Combust. Flame* **139**, 358–366 (2004).
- ²J. Geith, T. M. Klapötke, J. Weigand, and G. Holl, *Propellants, Explos., Pyrotech.* **29**, 3 (2004).
- ³J. Thiele and E. Uhlfelder, *Justus Liebigs Ann. Chem.* **303**, 93 (1898).
- ⁴J. J. Weigand, “High energy density materials based on tetrazole and nitramine compounds - Synthesis, scale-up and testing,” Ph.D. thesis (Ludwig-Maximiliian University of Munich, 2005).
- ⁵J. Liu, S. D. Chambreau, and G. L. Vaghjiani, *J. Phys. Chem. A* **115**, 8064 (2011).
- ⁶R. Sun, M. R. Siebert, L. Xu, S. D. Chambreau, G. L. Vaghjiani, H. Lischka, J. Liu, and W. L. Hase, *J. Phys. Chem. A* **118**, 2228 (2013).
- ⁷H. Kruse, L. Goerigk, and S. Grimme, *J. Org. Chem.* **77**, 10824 (2012).
- ⁸Y. Zhao and D. Truhlar, *Theor. Chem. Acc.* **120**, 215 (2008).
- ⁹M. Walker, A. J. A. Harvey, A. Sen, and C. E. H. Dessen, *J. Phys. Chem. A* **117**, 12590 (2013).
- ¹⁰T. H. Dunning, *J. Chem. Phys.* **90**, 1007 (1989).
- ¹¹R. A. Kendall, J. T. H. Dunning, and R. J. Harrison, *J. Chem. Phys.* **96**, 6796 (1992).
- ¹²H. Sun, P. Zhang, and C. K. Law, *J. Phys. Chem. A* **116**, 5045 (2012).
- ¹³J. M. L. Martin, *Chem. Phys. Lett.* **259**, 669 (1996).
- ¹⁴D. Feller and D. A. Dixon, *J. Chem. Phys.* **115**, 3484 (2001).
- ¹⁵P. Zhang, S. J. Klippenstein, and C. K. Law, *J. Phys. Chem. A* **117**, 1890 (2013).
- ¹⁶M. J. Frisch, G. W. Trucks, H. B. Schlegel, G. E. Scuseria, M. A. Robb, J. R. Cheeseman, J. J. A. Montgomery, T. Vreven, K. N. Kudin, J. C. Burant, J. M. Millam, S. S. Iyengar, J. Tomasi, V. Barone, B. Mennucci, M. Cossi, G. Scalmani, N. Rega, G. A. Petersson, H. Nakatsuji, M. Hada, M. Ehara, K. Toyota, R. Fukuda, J. Hasegawa, M. Ishida, T. Nakajima, Y. Honda, O. Kitao, H. Nakai, M. Klene, X. Li, J. E. Knox, H. P. Hratchian, J. B. Cross, C. Adamo, J. Jaramillo, R. Gomperts, R. E. Stratmann, O. Yazyev, A. J. Austin, R. Cammi, C. Pomelli, J. W. Ochterski, P. Y. Ayala, K. Morokuma, G. A. Voth, P. Salvador, J. J. Dannenberg, V. G. Zakrzewski, S. Dapprich, A. D. Daniels, M. C. Strain, O. Farkas, D. K. Malick, A. D. Rabuck, K. Raghavachari, J. B. Foresman, J. V. Ortiz, Q. Cui, A. G. Baboul, S. Clifford, J. Cioslowski, B. Stefanov, G. Liu, A. Liashenko, P. Piskorz, I. Komaromi, R. L. Martin, D. J. Fox, T. Keith, M. A. Al-Laham, C. Y. Peng, A. Nanayakkara, M. Challacombe, P. M. W. Gill, B. Johnson, W. Chen, M. W. Wong, C. Gonzalez, and J. A. Pople, *GAUSSIAN 09*, Revision D.01, Gaussian, Inc., Wallingford, CT, 2009.
- ¹⁷H.-J. Werner, P. J. Knowles, G. Knizia, F. R. Manby, M. Schütz, P. Celani, T. Korona, R. Lindh, A. Mitrushenkov, G. Rauhut, K. R. Shamasundar, T. B. Adler, R. D. Amos, A. Bernhardsson, A. Berning, D. L. Cooper, M. J. O. Deegan, A. J. Dobbyn, F. Eckert, E. Goll, C. Hampel, A. Hesselmann, G. Hetzer, T. Hrenar, G. Jansen, C. Köpli, Y. Liu, A. W. Lloyd, R. A. Mata, A. J. May, S. J. McNicholas, W. Meyer, M. E. Mura, A. Nicklaß, D. P. O'Neill, P. Palmieri, D. Peng, K. Pflüger, R. Pitzer, M. Reiher, T. Shiozaki, H. Stoll, A. J. Stone, R. Tarroni, T. Thorsteinsson, and M. Wang, *MOLPRO*, version 2012.1, a package of *ab initio* programs, 2012, see <http://www.molpro.net>.
- ¹⁸A. L. L. East and L. Radom, *J. Chem. Phys.* **106**, 6655 (1997).
- ¹⁹Y. Georgievskii and S. J. Klippenstein, *J. Chem. Phys.* **122**, 194103 (2005).
- ²⁰S. H. Robertson, M. J. Pilling, D. L. Baulch, and N. J. B. Green, *J. Phys. Chem.* **99**, 13452 (1995).
- ²¹H. S. Johnston and J. Heicklen, *J. Phys. Chem.* **66**, 532 (1962).
- ²²J. A. Miller and S. J. Klippenstein, *J. Phys. Chem. A* **110**, 10528 (2006).
- ²³A. Fernández-Ramos, J. A. Miller, S. J. Klippenstein, and D. G. Truhlar, *Chem. Rev.* **106**, 4518 (2006).
- ²⁴J. A. Miller and S. J. Klippenstein, *J. Phys. Chem. A* **107**, 2680 (2003).
- ²⁵S. J. Klippenstein, A. F. Wagner, R. C. Dunbar, D. M. Wardlaw, S. H. Robertson, and J. A. Miller, *VARIFLEX*, version 2.02m (Argonne National Laboratory, 2010).
- ²⁶B. E. Poling, J. M. Prausnitz, and J. P. O'Connell, *Properties of Gases and Liquids*, 5th ed. (McGraw-Hill Education, New York, Chicago, San Francisco, Athens, London, Madrid, Mexico City, Milan, New Delhi, Singapore, Sydney, Toronto, 2001).
- ²⁷J. O. Hirschfelder, C. F. Curtiss, and R. B. Bird, *Molecular Theory of Gases and Liquids* (Wiley, New York, 1954).
- ²⁸E. W. Hughes, H. Yakel, and H. C. Freeman, *Acta Crystallogr.* **14**, 345 (1961).
- ²⁹M. Suntova, I. Marochkin, and O. Dorofeeva, *Struct. Chem.* **24**, 745 (2013).
- ³⁰N. V. L. Yudin, D. A. Laktyuhin, and V. L. Zbarsky, in *New Trends in Research of Energetic Materials*, edited by J. Ottis and M. Krupka (University of Pardubice, Pardubice, Czech Republic, 2007), Vol. 10, p. 973.
- ³¹J. A. Miller and S. J. Klippenstein, *Phys. Chem. Chem. Phys.* **6**, 1192 (2004).
- ³²S. J. Klippenstein, L. B. Harding, P. Glarborg, Y. Gao, H. Hu, and P. Marshall, *J. Phys. Chem. A* **117**, 9011 (2013).
- ³³N. Lindholm and J. F. Hershberger, *J. Phys. Chem. A* **101**, 4991 (1997).
- ³⁴R. P. Saxon and M. Yoshimine, *J. Phys. Chem. A* **93**, 3130 (1989).
- ³⁵A. M. Mebel, C.-C. Hsu, M. C. Lin, and K. Morokuma, *J. Chem. Phys.* **103**, 5640 (1995).